

The performance of a multilevel multifunctional solar inverter under various control methods

Darshni M. Shukla¹, Naimish Zaveri¹, Tole Sutikno^{2,3}

¹Department of Electrical Engineering, Gujarat Technological University, Gujarat, India

²Department of Electrical Engineering, Universitas Ahmad Dahlan, Yogyakarta, Indonesia

³Embedded System and Power Electronics Research Group, Yogyakarta, Indonesia

Article Info

Article history:

Received May 19, 2022

Revised Aug 13, 2022

Accepted May 17, 2023

Keywords:

Conservative power theory

Instantaneous reactive power

Multilevel multifunctional

Solar inverter

Synchronous reference frame

ABSTRACT

Photovoltaic (PV) inverters are now supposed to provide additional supporting services with more reliability and efficiency. This paper presents three different control methods for generating reference current in a multifunctional, multilevel grid-tied PV inverter for harmonic, reactive, and unbalance compensation. These methods are the synchronous reference frame (SRF) theory (d-q), the instantaneous reactive power (IRP) theory (p-q), and the conservative power theory (CPT). As a result, the primary goal is to propose a low-cost multifunctional solar inverter for distributed generation, with an appropriate prototype developed in the laboratory for experimental validation of various modes of operation. Demonstrated results show that the presented inverter is capable of providing various ancillary services with all three types of control.

This is an open access article under the [CC BY-SA](#) license.



Corresponding Author:

Darshni M. Shukla

Department of Electrical Engineering, Gujarat technological University Gujarat

B 803, Dreamworld Residency, Canal Road, Vesu, Surat, Gujarat, India

Email: darshnishukla@yahoo.com

1. INTRODUCTION

Solar photovoltaic (SPV)-based renewable energy systems have gained worldwide acceptance because solar power is abundant and free [1]–[8]. To connect a photovoltaic (PV) source to the grid, two configurations are used. There are two stages: one stage and two stages. The single-stage SPV is directly integrated to the utility grid using an only DC to AC converter, while the double-stage SPV is integrated to the supply grid using a boost converter; both topologies are extensively discussed in [9]–[19]. However, single stage topology is now recommended because a boost converter is not required in this scheme, which not only reduces costs but also improves overall system efficiency. The presented system is a multi-functional H bridge-based inverter that addresses many issues encountered in distributed generation systems, such as energy shortage and poor power quality due to non-linear loads. The main advantages of H-bridge cascaded inverters are their upgradeable power rating, low cost, and modular structure [10], [20]–[27]. Apart from tracking point of maximum power and supplying generated electrical power to the utility grid, the proposed transformer-less single stage PV inverter can improve power quality.

The literature [28], [29] presented both two-stage grid and single-stage SPV systems. Both papers use solar inverters only for supply of active power into the utility grid. The literature [30], [31] present work that includes compensation of reactive power as well as active filtering, but load current balancing is not discussed, and hardware results are not provided. Research in [32], [33] proposed synchronous reference frame (SRF)-based control methods for grid-associated solar plants to improve power quality. Multiple functionalities in PV inverters play an significant role in lowering the complet cost of a solar plant due to

higher productivity and reliability. The overall efficiency of any PV system is determined by its ability to extract reference current signals. Control techniques for grid-connected solar PV include Akagies instantaneous reactive power (IRP) theory [34]–[39], SRF theory [40]–[48], leaky least mean square (LMS) [49], and LMS-least mean fourth (hybrid LMS-LMF) [50]–[52]. All of these theories proposed different methods for obtaining reference currents.

Many control techniques for inverters operating in standalone mode have also been presented in the literature. Singh and Solanki [53] presented a useful comparison of IRP theory, SRF, and Adaline-based LMS algorithms for DSTATCOM operation. The cascaded multilevel inverter is the most common configuration of multilevel inverters like the neutral point clamped (NPC) and flying capacitor multilevel inverters [54]–[59]. The cascaded multilevel inverter is made up of separate cascaded H-bridge (CHB) cells that are powered by individual solar panels. This paper proposed controlling a three-level three-phase grid-connected solar converter with separate voltage control of H-bridge DC-link in distribution-level operations. The proposed multi-functional inverter not only integrates generated electrical energy to the utility grid but also provides nighttime assistance, harmonic compensation, low voltage ride through (LVRT) support, and active anti-islanding detection capability. In this work, the performance and robustness of each control method of reference current generation are experimentally validated. The establishment of a transformerless, single-stage H bridge converter-based solar PV inverter with access to the grid is one of the study's contributions. Presented system is capable of providing very good controllable and manageable PV system integration into the distribution grid. Application of STM32 bit microcontroller to implement an adapted hysteresis control algorithm that includes all of the advantages of a hysteresis current controller while also maintaining a consistent switching frequency. This work presents a detailed comparative study for three most popular control strategies (d-q, p-q, and conservative power theory (CPT)) applied for reference generation. Any of these techniques can be used to solve a specific power quality problem with the STM32 bit microcontroller. Active islanding detection and LVRT support are implemented for the grid-integrated multifunctional converter to provide a cost-effective solution to low and medium voltage industrial loads. The proposed system's feasibility is demonstrated using real-time experimental results.

2. METHOD

Figure 1 presents a line diagram for the proposed system. The proposed configuration uses a single-stage, transformerless, three-level, multipurpose photovoltaic inverter coupled with the distribution grid and the point of common coupling of a non-linear load. Here, the voltage of each of the three H bridge cells have been controlled by three proportional integral (PI) controllers. An inverter turns on and a hysteresis current controller regulates the current. The perturb and observe (P&O) maximum power point tracking (MPPT) approach is used to extract the maximum power available from solar panel. The grid synchronisation is done by employing second-order generalised integrator (SOGI) estimators. Three algorithms d-q/p-q/CPT are employed for producing reference signal. In this work, a diode rectifier with resistive load at the output yields a nonlinear load.

2.1. Reference signal generation on the basis of instantaneous reactive power theory

Akagi was the first person to put forward this concept [60]. This theory suggests that in order to calculate active and reactive power in this frame, three-phase instantaneous values must initially be converted into two-phase values in a stationary reference frame using the Clark transformation [60]. The block diagram for this theory is given in Figure 2. Grid voltages U_a , U_b , U_c and load currents i_{La} , i_{Lb} , i_{Lc} are sensed and fed to the controller for processing and generating the reference currents i_a^* , i_b^* , i_c^* . These currents are compared with actual inverter currents i_a , i_b , i_c by hysteresis current controller as shown and switching signals are produced. As a result, the block in figure will be used as the figure controller block. The block diagram of p-q control in Figure 2 generates three-phase instantaneous grid voltages.

$$u_{sa} Um \sin \omega t \quad (1)$$

$$u_{sb} Um \sin \omega t - \frac{2\pi}{3} \quad (2)$$

$$u_{sc} Um \sin \omega t + \frac{2\pi}{3} \quad (3)$$

And the load current is represented by:

$$i_{la} = \sum i_{Lan} \sin\{n(\omega t) - \theta_{an}\} \quad (4)$$

$$i_{lb} = \sum i_{Lbn} \sin\left\{n(\omega t - \frac{2\pi}{3}) - \theta_{bn}\right\} \quad (5)$$

$$i_{lc} = \sum i_{Lcn} \sin\left\{n(\omega t + \frac{2\pi}{3}) - \theta_{cn}\right\} \quad (6)$$

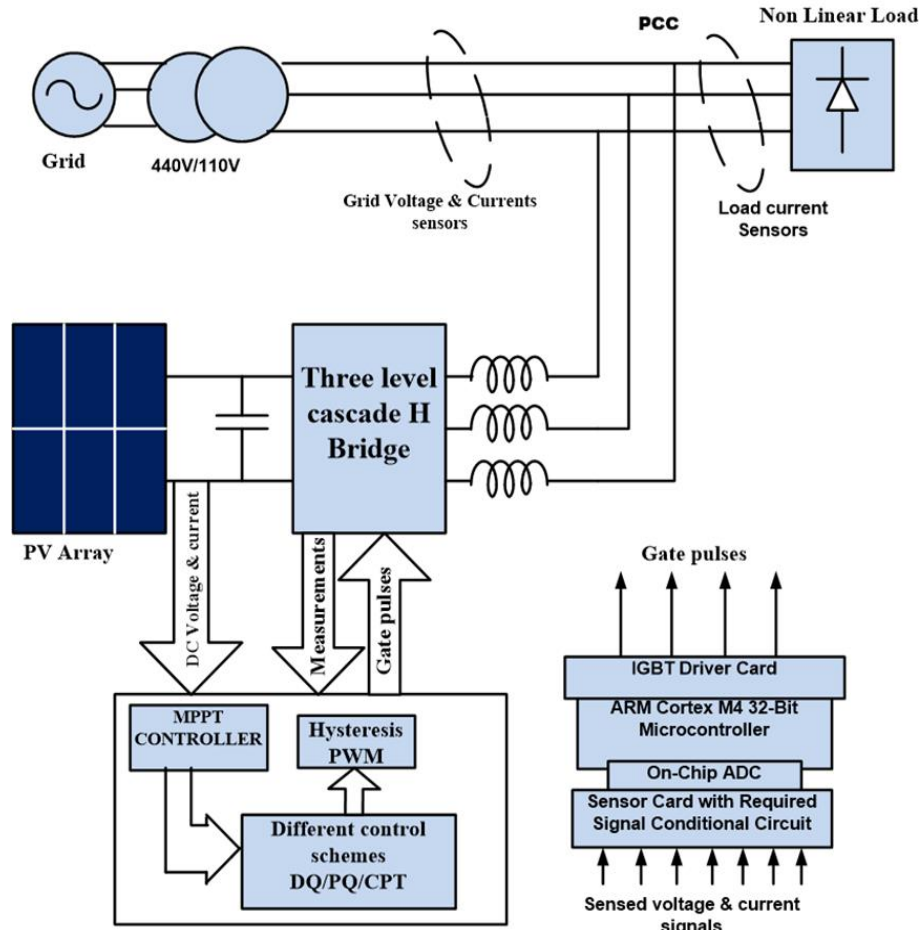


Figure 1. Block diagram of presented system

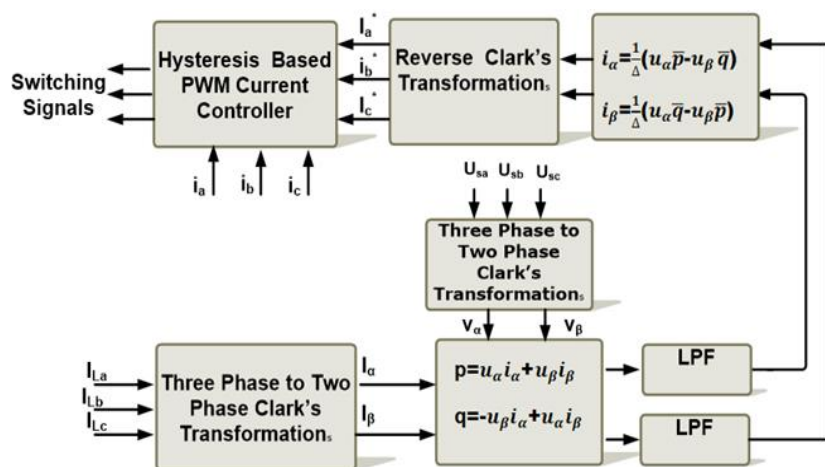


Figure 2. Reference current extraction in p-q theory

As shown here, the instantaneous phasors of the grid voltage and load currents can be simultaneously transformed into stationary frames using the Clark's transformation.

$$\begin{bmatrix} u_\alpha \\ u_\beta \end{bmatrix} = \sqrt{\frac{3}{2}} \begin{bmatrix} 1 & -\frac{1}{2} & -\frac{1}{2} \\ 0 & -\frac{\sqrt{3}}{2} & -\frac{\sqrt{3}}{2} \end{bmatrix} \begin{bmatrix} u_{sa} \\ u_{sb} \\ u_{sc} \end{bmatrix} \quad (7)$$

$$\begin{bmatrix} i_\alpha \\ i_\beta \end{bmatrix} = \sqrt{\frac{3}{2}} \begin{bmatrix} 1 & -\frac{1}{2} & -\frac{1}{2} \\ 0 & -\frac{\sqrt{3}}{2} & -\frac{\sqrt{3}}{2} \end{bmatrix} \begin{bmatrix} i_{La} \\ i_{Lb} \\ i_{Lc} \end{bmatrix} \quad (8)$$

Now representation of instantaneous power in the conventional three-phase circuit as in (9):

$$p = u_a * i_a + u_b * i_b + u_c * i_c \quad (9)$$

The real and reactive power have been defined as follows in the IRP theory:

$$p = u_\alpha * i_\alpha + u_\beta * i_\beta \quad (10)$$

$$q = -u_\beta * i_\alpha + u_\alpha * i_\beta \quad (11)$$

Real power (p), imaginary power (q), and zero-sequence power (p_0) all three instantaneous powers, can be determined from line currents and instantaneous phase voltages in $\alpha\beta0$ coordinates as in (12):

$$\begin{bmatrix} p_0 \\ p \\ q \end{bmatrix} = \begin{bmatrix} u_0 & 0 & 0 \\ 0 & u_\alpha & u_\beta \\ 0 & u_\beta & -u_\alpha \end{bmatrix} \begin{bmatrix} i_0 \\ i_\alpha \\ i_\beta \end{bmatrix} \quad (12)$$

Instantaneous active and reactive powers p and q result from both an oscillatory component and an average component.

$$(p = \bar{p} + \check{p}) \text{ and } (q = \bar{q} + \check{q}) \quad (13)$$

By calculating the appropriate reference source currents, the oscillatory component of the instantaneous active power and the IRP are compensated. It's important for the source to only supply the active power's non-oscillating component. In (14) can be used to calculate $\alpha\beta$ currents:

$$\begin{bmatrix} i_{s\alpha}^* \\ i_{s\beta}^* \end{bmatrix} = \frac{1}{\sqrt{u_\alpha^2 + u_\beta^2}} \begin{bmatrix} u_\alpha & -u_\beta \\ u_\beta & u_\alpha \end{bmatrix} \begin{bmatrix} \bar{p} \\ 0 \end{bmatrix} \quad (14)$$

Then, using inverse Clark transformations, these currents are transferred into the a-b-c frame as shown in (15):

$$\begin{bmatrix} i_a^* \\ i_b^* \\ i_c^* \end{bmatrix} = \sqrt{\frac{2}{3}} \begin{bmatrix} \frac{1}{\sqrt{2}} & 1 & 0 \\ \frac{1}{\sqrt{2}} & -\frac{1}{2} & \frac{\sqrt{3}}{2} \\ \frac{1}{\sqrt{2}} & -\frac{1}{2} & -\frac{\sqrt{3}}{2} \end{bmatrix} \begin{bmatrix} i_0^* \\ i_{s\alpha}^* \\ i_{s\beta}^* \end{bmatrix} \quad (15)$$

2.2. Synchronous reference frame theory

The idea has been laid out by [61], which suggests the transformation of voltage and currents on a reference frame which rotates synchronously. A block diagram of this concept is shown in Figure 3. The controller receives the sensed input voltages U_a , U_b , U_c as well as currents i_{La} , i_{Lb} , i_{Lc} . According to this theory, phase locked loop (PLL) needs to be cognizant of the grid voltages' angle. For the required active and reactive references, load currents are transferred into the d-q frame and decoupled into the d and q axes, and then transmitted again to the instantaneous a-b-c frame to supply the hysteresis current controller. After converting current components in the stationary frame ($\alpha\beta0$) using θ angle, these currents are subsequently transformed from - to d-q frames using (Park's transformation).

$$\begin{bmatrix} i_a \\ i_q \end{bmatrix} = \begin{bmatrix} \cos \theta & \sin \theta \\ -\sin \theta & \cos \theta \end{bmatrix} \begin{bmatrix} i_a \\ i_\beta \end{bmatrix} \quad (16)$$

The synchronous frame produces DC current values by rotating at a constant speed in synchronisation with the instantenous a-b-c voltages. The fundamental positive sequence components of the load currents in a synchronously rotating reference frame are represented by their constant part, which has been eliminated by a low-pass filter from the load currents in a synchronously rotating reference frame. Finally, those components have been transferred from the d-q frame to the a-b-c frame using (17).

$$\begin{bmatrix} i_{\alpha dc} \\ i_{\beta dc} \end{bmatrix} = \begin{bmatrix} \cos \theta & \sin \theta \\ -\sin \theta & \cos \theta \end{bmatrix} \begin{bmatrix} i_{ddc} \\ i_{qdc} \end{bmatrix} \quad (17)$$

The inverse transformation is then performed using (18) to yield three-phase reference source currents in a, b, and c coordinates.

$$\begin{bmatrix} i_{ca}^* \\ i_{cb}^* \\ i_{cc}^* \end{bmatrix} = \begin{bmatrix} \sin \omega t & \cos \omega t & 1 \\ \sin \left(\omega t - \frac{2\pi}{3} \right) & \cos \left(\omega t - \frac{2\pi}{3} \right) & 1 \\ \sin \left(\omega t + \frac{2\pi}{3} \right) & \cos \left(\omega t + \frac{2\pi}{3} \right) & 1 \end{bmatrix} \begin{bmatrix} i_{cd}^* \\ i_{cq}^* \\ i_{co}^* \end{bmatrix} \quad (18)$$

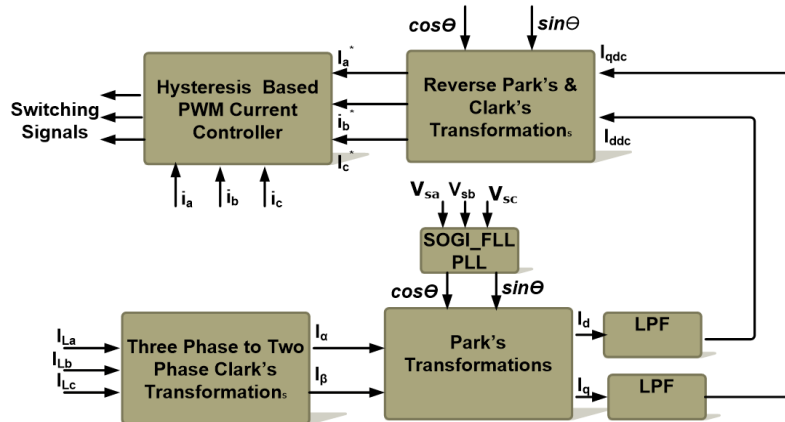


Figure 3. Block diagram of d-q control

2.3. Conservative power theory

CPT was first developed by [62] and subsequently modified [63], [64]. Many researchers have focused on CPT in grid-connected inverter control applications and active power conditioners. In CPT, selective compensation is accomplished by orthogonally isolating undesirable current components. A CPT algorithm implementation does not necessitate any reference frame translation aside from this. Although the CPT, which operates within a time-domain framework, is capable of handling polyphase systems, this work is focused on three-phase and three-wire systems. Consider the m phase network where u is vector of phase voltage, i is vector of phase current and \hat{u} is vector of unbiased voltage which is given by $\hat{u}=\omega(u_l-\hat{u}_l)$ here $u_l = \int_0^t u(\tau) d\tau$ $\hat{u} = \int_0^t u dt$ and $\omega = 2\pi f$ f is frequency and T is time period [62]. The following conservative quantities are defined as:

- The instantaneous power $p=u \cdot i$
- The instantaneous reactive energy $w=\hat{u} \cdot i$
- The active power $P=\bar{p}=\langle u, i \rangle$
- The reactive energy $E=\bar{e}=\langle \hat{u}, i \rangle$
- Here \cdot is scalar product and $\langle \rangle$ is inner product

According to CPT, the active currents can be separated from the load current.

$$i_{am} = \frac{(u_m i_m)}{\|u\|_2} u_m = \frac{P_m}{u_m^2} U_m = G_m U_m \quad (19)$$

The equivalent conductance in this case is the reactive phase currents (G_m).

$$i_{rm} \frac{(\widehat{u_m} i_m)}{\|u_m\|^2} \widehat{u_m} = \frac{Em}{u_m^2} \widehat{u_m} = B_m \widehat{u_m} \quad (20)$$

Where (B_m) is the equivalent phase reactivity. The remaining currents are void current \underline{i}_{vm} and are determined by subtracting active and reactive current from the total phase current as given as in (21):

$$\underline{i}_{vm} = \underline{i}_m - \underline{i}_{am} - \underline{i}_{rm} \quad (21)$$

Balance active current is subsequently supplied by current.

$$\underline{i}_{am}^b = \frac{(v,i)}{\|u\|^2} u_m = \frac{P}{v^2} u_m = G^b \underline{u}_m \quad (22)$$

The defined balanced reactive currents include in (23):

$$\underline{i}_{rm}^b = \frac{(\widehat{u},i)}{\|\widehat{u}\|^2} \widehat{u}_m = \frac{E}{\widehat{u}^2} u_m = B^b \underline{\widehat{u}}_m \quad (23)$$

Unbalanced active currents are obtained by subtracting the total active current from the balance active current.

$$i_{am}^w = i_{am} - i_{am}^b = (G_m - G^b) u_m \quad (24)$$

The imbalanced reactive currents are created similarly as in (25):

$$i_{rm}^w = i_{rm} - i_{rm}^b = (B_m - B^b) \widehat{u}_m \quad (25)$$

I_m^w which is the total imbalance phase current, is therefore determined in (26):

$$I_m^w = I_{am}^w + I_{rm}^w \quad (26)$$

The measured current vector may be divided into four separate components as shown in (27):

$$\underline{i} = \underline{i}_a b + \underline{i}_r b + \underline{i}_a u + \underline{i}_r u \quad (27)$$

However, as previously stated definitions stated all of the current's components are orthogonal to one another, hence the RMS value is shown as in (28):

$$I = \sqrt{I_a^b + I_r^b + I_a^w + I_r^w + I_v^2} \quad (28)$$

Similar to that, apparent power (Pa) is described as:

$$P_a = \|u\| \cdot \|i\|$$

$$P_a = \|v\| \cdot \sqrt{I_a^b + I_r^b + I_a^w + I_r^w + I_v^2} \quad (29)$$

or

$$P_a = \sqrt{P^2 + Q^2 + N_a^2 + N_r^2 + D^2} \quad (30)$$

Where active power is $P = UI_a^b$, reactive power is $Q = UI_r^b$, unbalanced active power is $N_a = UI_a^u$, unbalanced reactive power is $N_r = UI_r^u$, and distortion power is $D = UI_v$.

This theory states that several variables in (28) that are applicable to power conditioning applications are independent of the current and voltage waveforms of the circuit. The existence of periodic quantities is the sole requirement. The formation of various compensating currents using the CPT algorithm is illustrated in Figure 4.

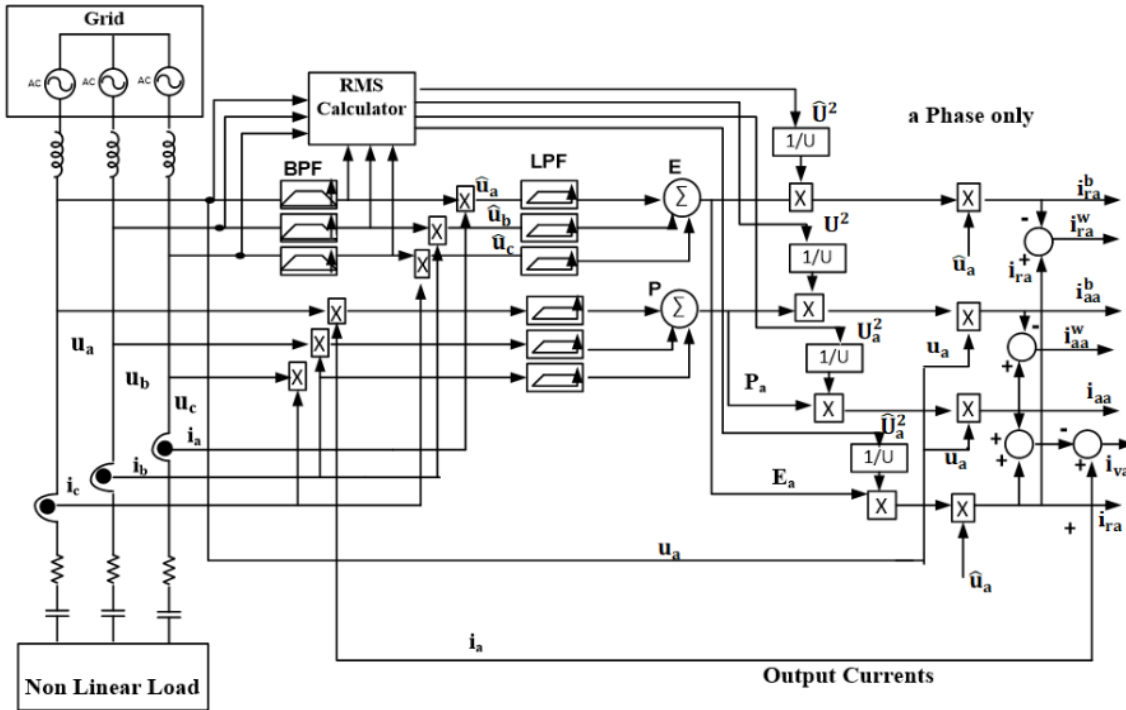


Figure 4. Reference current extraction in CPT

2.4. Voltage and current control implementation

This section describes how the proposed grid-connected inverter, which is depicted in Figure 1, would put the control method into effect. Since there are three CHB employed here (one for each phase), there are three different DC-links, MPPT is used, their average is regulated. The outer loop controls the DC-link voltage. The P&O approach is used for sampling the outer loop every 0.001 seconds in order to monitor the maximum power point. Combining SOGI-frequency locked loop (FLL) and DC blockers, just one voltage sensor is needed for grid angle determination. For the outer voltage control loop, the PI values for the proportional controller (K_p) and integral controller (K_i) gains are kept at 0.3 and 0.2, respectively. In this study, a modified hysteresis current control approach is used to switch and control a three-phase, three-level inverter. A signal is acquired, compared, and the switching pattern is adjusted according to requirement at the end of each sample period, 50 samples are taken each microsecond as the sampling rate. Instead of comparing actual and reference currents in a real experimental prototype, current error was used. Additionally, in order to maintain a consistent switching frequency, 10 microseconds dead time are added between two successive changing switching patterns, during which all the switches are switched off.

2.5. Multifunctional operations mode of inverter

A flowchart describing the proposed inverter's multifunctional operation mode is shown in Figure 5. The inverter being demonstrated has six different modes of operation. In daylight PV mode, it will simultaneously provide the grid with active electricity generated by PV along with power factor correction and harmonics elimination caused by nonlinear load, active filtering, and power factor correction mode. In this PV mode, it will use the remaining capacity to provide reactive energy to the grid. Throughout the night, it will operate at full capacity to offer reactive support to the grid. The negligible amount of active energy necessary to maintain a DC link will be supplied by the grid. If the grid voltage drops below 70% of its nominal value, reactive power will start to assist the grid until it reaches maximum capacity. The LVRT capacity of the inverter refers to the ability to stop supplying active power this time. The grid will instantly stop feeding the grid and enter islanding mode if it is suddenly disconnected.

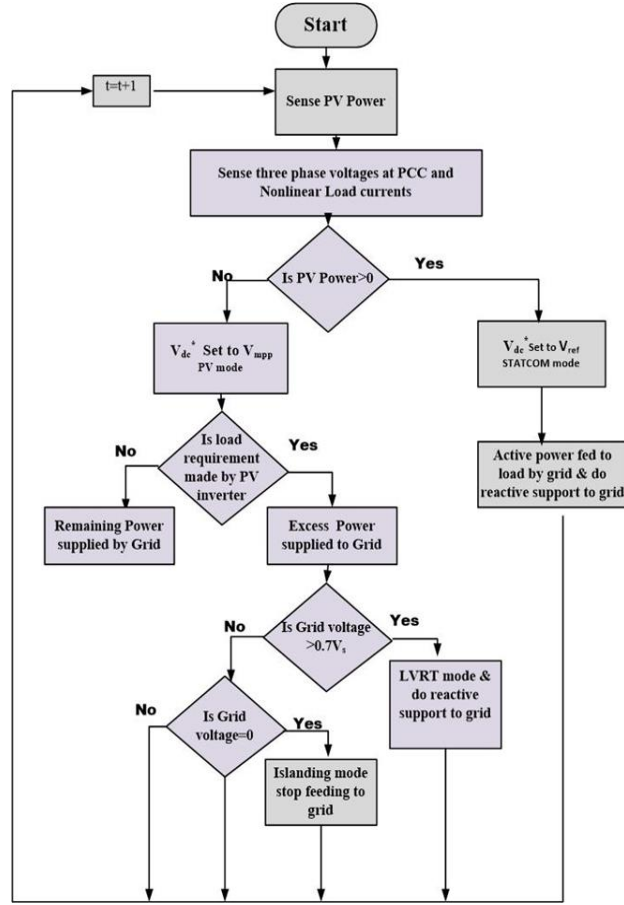


Figure 5. Flowchart for multifunctional operation modes

2.6. Experimental setups

A prototype has been developed in a lab for the proposed system's real-time implementation; Figure 6 depict the image of this prototype. The nonlinear load (MDS 100) and the three-level, three-phase H-bridge solar inverter are both directly linked to the 230 V supply grid. Three inductors with a value of 6 mH are implemented as line inductors, and the inverter is controlled by an ARM cortex-M4 microcontroller (STM32F407VG). A single-phase, four-switch insulated gate bipolar transistor (IGBT) inverter module and two 150 Wp SPV sources comprise each phase of an H-bridge PV inverter. An inductive current transformer detects the grid voltage, load current, and grid currents. Both the DC-bus voltage and solar PV current are detected by a sensor card that depends on the hall effect. Table 1 provides specific details about real-time implementations.

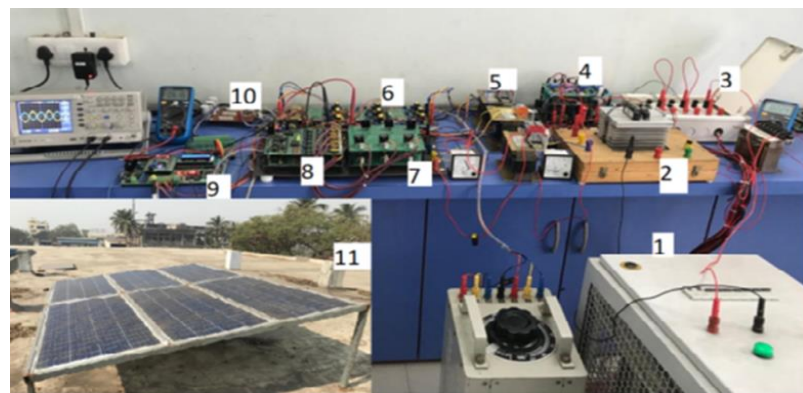


Figure 6. Experimental setup

Table 1. Details of components used in experimental setup

Parameter/component	Value
SPV source	150 Wp (waaree energies Ltd) 44.30 V
Open circuit voltage (Voc)	4.51 A
Short circuit current (Isc)	36.10 V
Voltage at maximum power (Vm)	4.16 A
Current at maximum power (Im)	1000 V
Maximum system voltage module efficiency (%)	12.89
PV capacity	900 W
Grid supply	400 V, 50 Hz
Auto-transformer rating (line voltage, current)	400 V/130 V, 15 A
Line inductor	6 mH
IGBT inverter module:	5 KW (600 V/1200 V, 25 A IGBTs)
Ripple Fi	5 Ω 10 W, 2.5 μF/440 V
lter (Rf, Cf)	
Non-linear load (diode bridge rectifier)	MDS100/04 400 V
Kp, Ki values	0.3, 0.2
DC-link capacitor	4700 mF 450 V (single on each DC LINK)

3. RESULTS AND DISCUSSION

Employing three different approaches for reference current generation, the performance of the suggested solar PV inverter in the multifunctional operating mode is monitored in real time. As seen in Figures 7(a)-(c), as well as Figures 8(a)-(c), the inverter operation in this work incorporates soft start and soft stop. Switching strains, losses, and noise were greatly decreased with the use of soft switching. These figures show how smoothly the inverter pulse width modulation (PWM) operations and switching transition proceed. When the nonlinear load varies, Figures 9(a)-(c) demonstrate the active filtering operation of the given inverter in multifunctional mode for all three techniques for reference current generation. The figures make it evident that the suggested H-bridge inverter can properly compensate for harmonics produced by a nonlinear load with all three methods since the source current is sinusoidal which is clear from results shown.

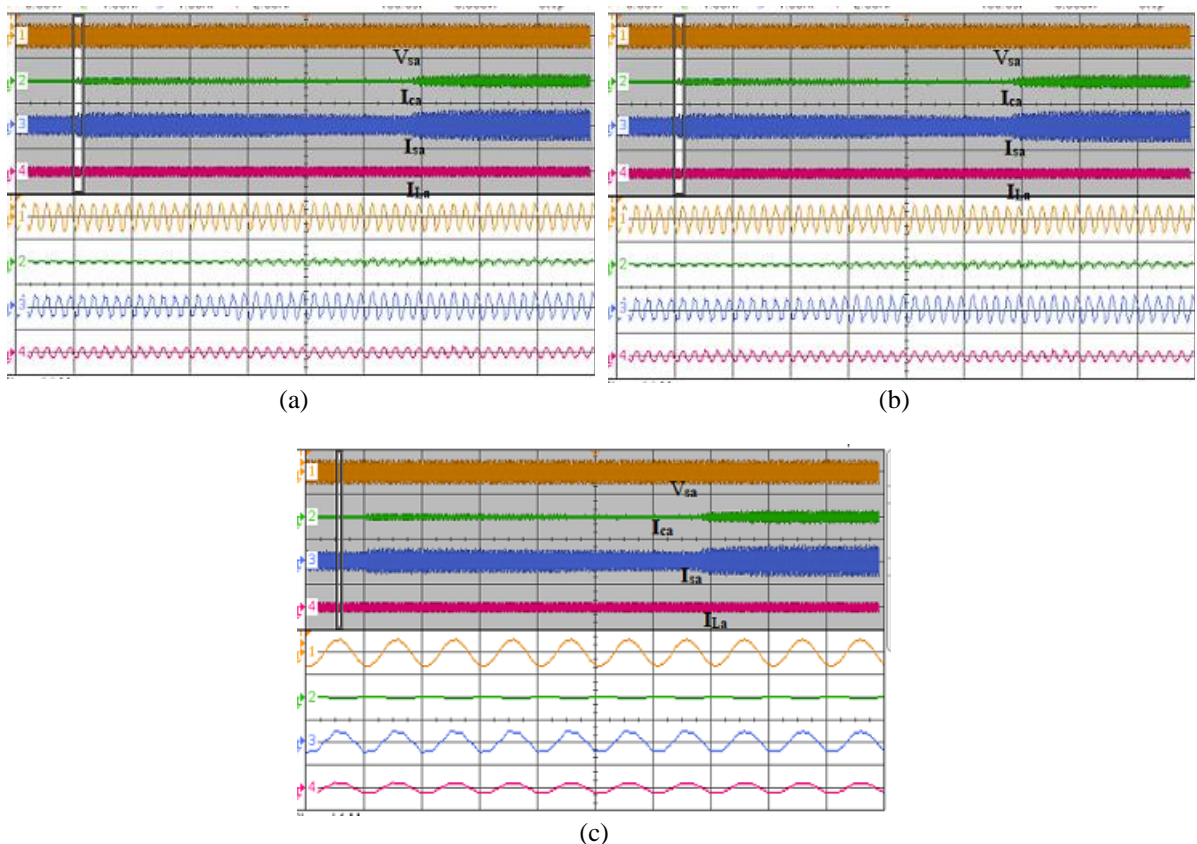


Figure 7. Soft start in multifunctional operation of inverter (a) d-q, (b) p-q, and (c) CPT.

Scale-horizontal 50 ms/div & 5 s/div vertical Vsa=50V/div, Ica, Isa, ILa=2 A/div

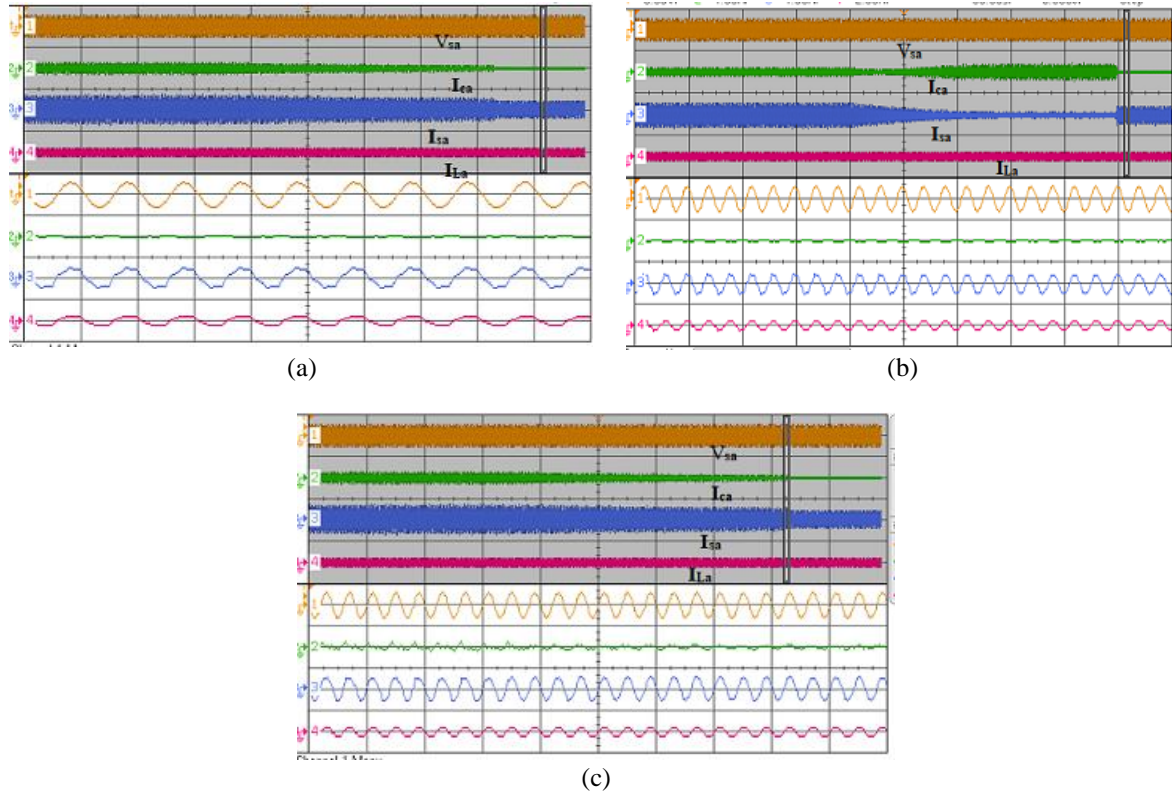


Figure 8. Soft stop in multifunctional operation of inverter (a) d-q, (b) p-q, and (c) CPT.
Scale-horizontal 50 ms/div & 5 s/div vertical Vsa=50V/div, Ica, Isa, ILa=2 A/div

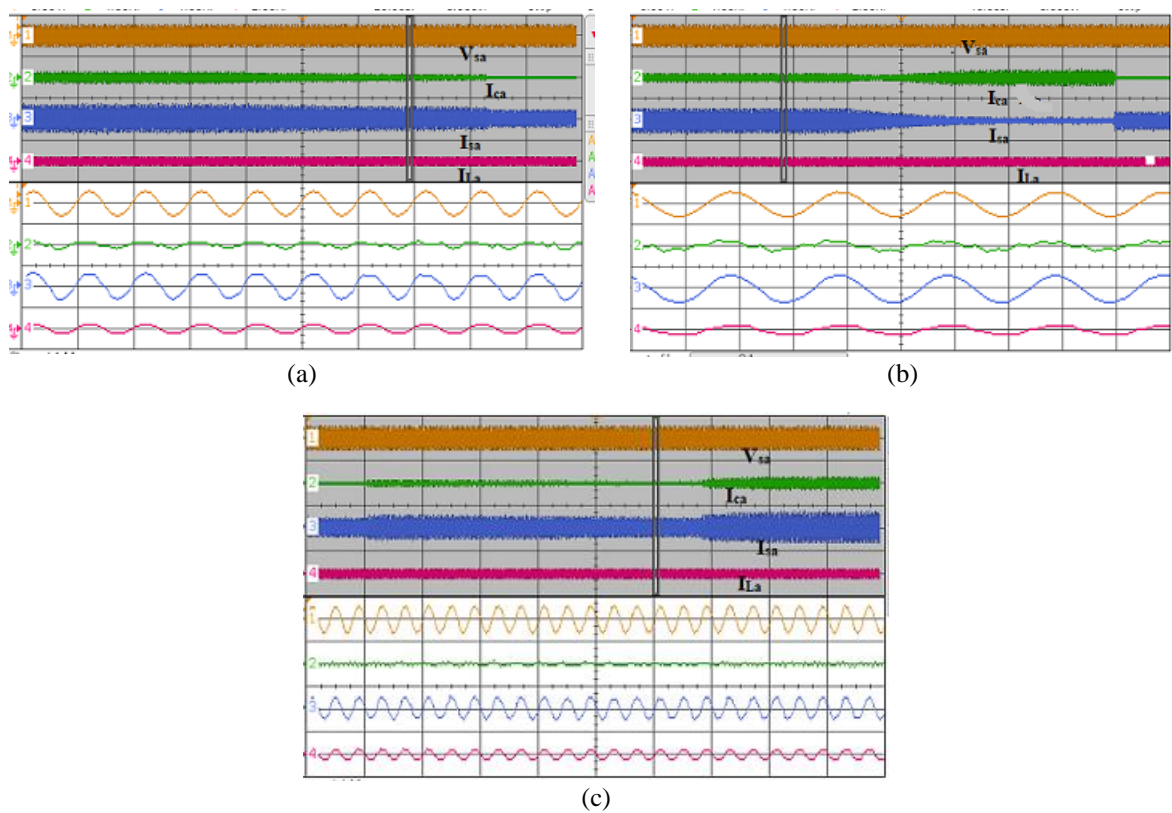


Figure 9. Active filtering in multifunctional operation of inverter (a) d-q, (b) p-q, and (c) CPT.
Scale-horizontal 20 ms/div & 5 s/div vertical Vsa=50V/div, Ica, Isa, ILa=2 A/div

The dynamic performance of the inverter for each of the three reference generation controls can be observed in Figures 10(a)-(c) when the load current is gradually raised from 1.7 A to 3.7 A and subsequently lowered to 0.66 A. The grid current's fast fourier transform (FFT) is illustrated in Figures 11(a)–(f) both before and after active filtering. The inverter can compensate for third, fifth, and other harmonics and make the injected current nearly sinusoidal, as shown by the figures. With CPT control, performance is improved. Based on the experiment's outcomes, the inverter can satisfy load demand while also successfully carrying out active filtering and power factor modifications functions.

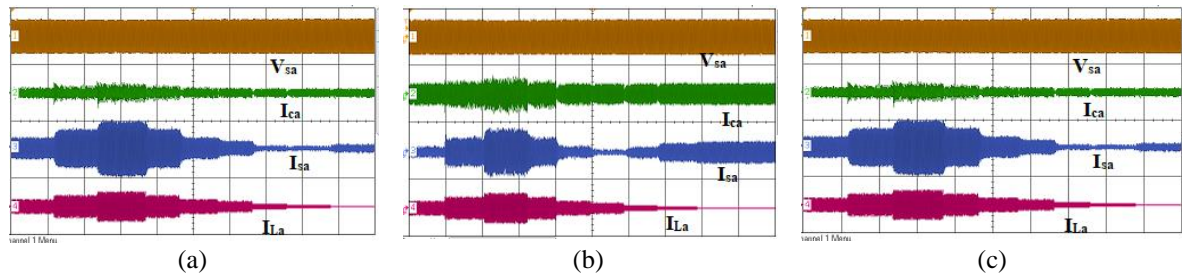


Figure 10. Dynamic performance of inverter for changing load (a) d-q, (b) p-q, and (c) CPT.
Scale-horizontal 5 s/div vertical $V_{sa}=50V/div$, $I_{ca}, I_{sa}=2 A/div$

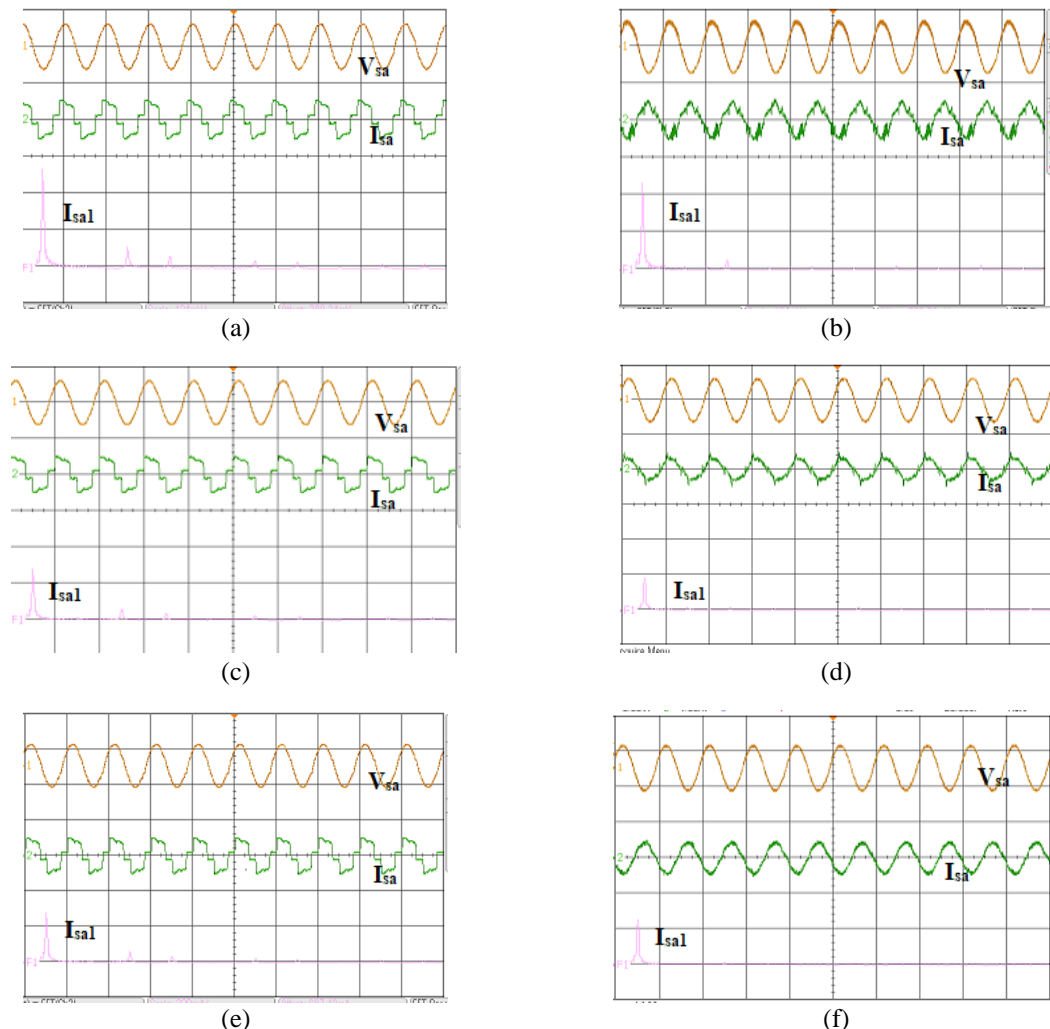


Figure 11. FFT of grid current in all three-reference current generation (a) d-q before active filtering, (b) d-q after application of active filtering, (c) p-q before active filtering, (d) p-q after application of active filtering, (e) CPT before active filtering, and (f) CPT after application of active filtering

Figures 12(a)-(b), which depict the low-voltage ride through and islanding modes, respectively. Figure 12(a) makes it clearly apparent that the inverter directs I_q currents to rise when it detects low voltage on the grid in order to continue providing reactive power on the grid. In the meanwhile, V_d commands drop to indicate that the inverter no longer supplies the grid any active power. The system of operation for islands is illustrated in Figure 12(b). Figure 12(b) illustrates how the inverter enters islanding mode and stops feeding when the grid voltage approaches 70% of its nominal value. The result is demonstrated by the decline in the V_d command vector. Figures 13(a)-(b) depict an inverter's power factor modification mode for low and high value of current. Here, the power factor modification capacity of the presented inverter is taken into consideration in conjunction with the grid voltage (V) and injected current (I). Given that the inverter is injecting extra power into the grid, it is evident from the two numbers that grid voltage and grid current are in 1800-phase opposition to each other.

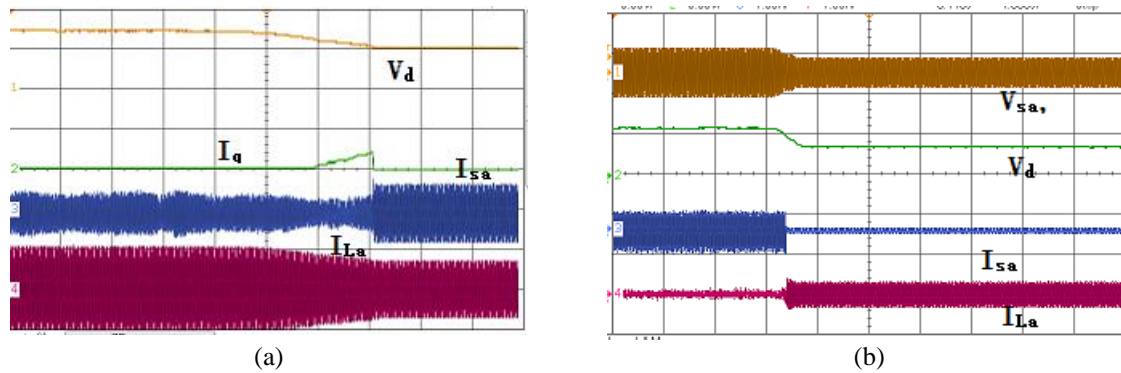


Figure 12. These figure are, (a) LVRT mode and (b) islanding mode

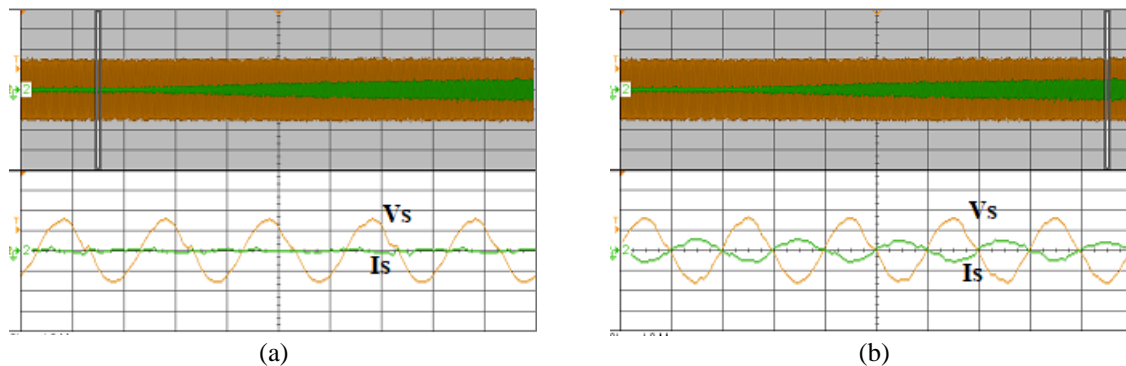


Figure 13. Power factor correction mode of inverter, (a) low value of current and (b) high value of current

Three different techniques for producing reference current for inverter control are employed in this study and brought to the test experimentally. PI controllers are typically used in SRF (dq) control strategies, however in grid-connected applications, these controllers have very poor low-order harmonic compensation capabilities. The low-pass filters utilised in this approach for filtering signals in the d-q frame for the extraction of reference current cause a delay in response that also appears. The generation of the sine and cosine voltage templates is crucial for calculating reference source currents. Proportional-resonant (PR) controllers are employed in the IRP (p-q) control method. Lower-order harmonics are easier to regulate using PR controllers in the stationary reference frame than higher-order harmonics the SRF. Additionally, just the filtered grid voltage is needed for the generation of the current reference; there is no need to figure out the grid voltage's phase angle. To compute instantaneous active and reactive powers. However, IRP theory requires voltage signals; voltage imbalance or distortion will lead to inaccurate estimation of reference source currents. Actually, all that is required is the load current's accurate value at fundamental frequency component. A hysteresis current controller rather than a PI/PR controller is employed in this study. The primary drawback of this controller is the requirement for a variable switching frequency and a very high

sampling rate in order to get the best possible outcomes. An arm cortex microcontroller with constant frequency hysteresis control is used to fix these issues. A signal is acquired at the ending of each sample period, compared, and the switching pattern is adjusted appropriately. Also, a dead time of a few microseconds is inserted here between the changing switching patterns.

This maintains a 20 kHz switching frequency. Additionally, unlike the PI and PR controllers, this technique does not require a modulator. This controller features constant switching frequency, quick dynamic response, simplicity, stability, load parameter independence, quick transient response, and robustness. Because output current must always be in phase to operate at unity power factor or at a certain displacement angle to support voltage (when using LVRT or high voltage ride through (HVRT)), grid synchronisation is essential. In accordance with the IEEE 1547 draught regulation, the SOGI demonstrates extremely excellent dynamics under disrupted grid voltage situations and offers good reactive assistance during an LVRT event. Reference current generation based on CPT offers greater flexibility and selective compensation. These control techniques can be used to control instantaneous vectors a-b-c without the need for any reference-frame transformations. This approach works because it only causes substantial changes with the specified current disturbances. Thus, a key component of the CPT-based method is selecting the proper portions to be compensated. Table 2 presents an assessment of the three algorithms performance for the creation of the reference current complying with the results of the experiment.

Table 2. Comparative study of performance all three algorithm for reference current generation

Parameter	SRF theory	IRP theory	CPT
Number of maths operations	More	Least	Highest
Total harmonics distortion in grid current	Average	Better	Slight better
Reference frame transformation	Yes	Yes	No
Selective compensations	No	No	Yes
Multifunctional operations	Possible	Possible	Possible
Number of instructions in processor	Less	Least	Highest

4. CONCLUSION

The experimental outcomes demonstrate that the system's performance in its present state meets the requirements for active power injection with maximum power extraction, power factor correction, reactive power compensation, harmonic elimination, LVRT support, and islanding detection. The newly proposed approach outperforms all three of the current reference generations in terms of the response time of the system. By employing soft start and soft stop along with constant frequency hysteresis current control, losses and stress in devices can be minimized. Therefore, these devices are more suitable for converters with modules that are utilised in distribution-level applications. Because all of the results provided here were acquired in real time without making use of expensive processors and inverters. This work suggests a low-cost option for medium-voltage applications in both urban and rural settings. Both urban and rural locations can use this method. With the multifunctional inverter that has been developed as a result of this research, less number of individual devices will be required to accomplish a variety of applications.

REFERENCES

- [1] K. -D. Jäger, O. Isabella, A. H. M. Smets, R. A. C. M. M. v. Swaaij, and M. Zeman, *Solar energy: fundamentals, technology, and systems*. Cambridge: UIT Cambridge, 2014.
- [2] S. E. Halledj and A. Bouafassa, "Anti-disturbance GITSMC with quick reaching law for speed control of PMSM drive," *Bulletin of Electrical Engineering and Informatics*, vol. 11, no. 6, pp. 3228–3238, 2022, doi: 10.11591/eei.v11i6.4222.
- [3] L. T. Thang, T. V. Son, T. D. Khoa, and N. X. Chiem, "Synthesis of sliding mode control for flexible-joint manipulators based on serial invariant manifolds," *Bulletin of Electrical Engineering and Informatics*, vol. 12, no. 1, pp. 98–108, 2023, doi: 10.11591/eei.v12i1.4363.
- [4] M. Belkacem, K. Z. Meguenni, and I. K. Bousserhane, "Comparative study between backstepping and backstepping sliding mode controller for suspension of vehicle with a magneto-rheological damper," *International Journal of Power Electronics and Drive Systems*, vol. 13, no. 2, pp. 689–704, 2022, doi: 10.11591/ijpeds.v13.i2.pp689-704.
- [5] T. D. Chuyen *et al.*, "Improving control quality of PMSM drive systems based on adaptive fuzzy sliding control method," *International Journal of Power Electronics and Drive Systems*, vol. 13, no. 2, pp. 835–845, 2022, doi: 10.11591/ijpeds.v13.i2.pp835-845.
- [6] T. Someswari, A. K. Tiwari, and R. Nagraj, "Dynamic cruise control system for effective navigation system," *International Journal of Electrical and Computer Engineering*, vol. 10, no. 5, pp. 4645–4654, 2020, doi: 10.11591/ijece.v10i5.pp4645-4654.
- [7] D. Meradi, Z. A. Benselama, and R. Hedjar, "A predictive sliding mode control for quadrotor's tracking trajectory subject to wind gusts and uncertainties," *International Journal of Electrical and Computer Engineering*, vol. 12, no. 5, pp. 4861–4875, 2022, doi: 10.11591/ijece.v12i5.pp4861-4875.
- [8] K. O. Omali, M. N. Kabbaj, and M. Benbrahim, "Fault-tolerant control with high-order sliding mode for manipulator robot," *International Journal of Power Electronics and Drive Systems*, vol. 13, no. 3, pp. 1854–1869, 2022, doi: 10.11591/ijpeds.v13.i3.pp1854-1869.

[9] T.-F. Wu, C.-H. Chang, L.-C. Lin, and C.-L. Kuo, "Power loss comparison of single-and two-stage grid-connected photovoltaic systems," *IEEE Transactions on Energy Conversion*, vol. 26, no. 2, pp. 707–715, 2011, doi: 10.1109/TEC.2011.2123897.

[10] T. Sutikno, H. S. Purnama, R. A. Aprilianto, A. Jusoh, N. S. Widodo, and B. Santosa, "Modernisation of DC-DC converter topologies for solar energy harvesting applications: a review," *Indonesian Journal of Electrical Engineering and Computer Science*, vol. 28, no. 3, pp. 1845–1872, 2022, doi: 10.11591/ijeecs.v28.i3.pp1845-1872.

[11] M. Nivas, R. K. P. R. Naidu, D. P. Mishra, and S. R. Salkuti, "Modeling and analysis of solar-powered electric vehicles," *International Journal of Power Electronics and Drive Systems*, vol. 13, no. 1, pp. 480–487, 2022, doi: 10.11591/ijpeds.v13.i1.pp480-487.

[12] K. Kommuri and V. R. Kolluru, "Implementation of modular MPPT algorithm for energy harvesting embedded and IoT applications," *International Journal of Electrical and Computer Engineering*, vol. 11, no. 5, pp. 3660–3670, 2021, doi: 10.11591/ijece.v11i5.pp3660-3670.

[13] D. P. Mishra, R. Senapati, and S. R. Salkuti, "Comparison of DC-DC converters for solar power conversion system," *Indonesian Journal of Electrical Engineering and Computer Science*, vol. 26, no. 2, pp. 648–655, 2022, doi: 10.11591/ijeecs.v26.i2.pp648-655.

[14] S. Ramamurthi and P. Ramasamy, "High step-up DC-DC converter with switched capacitor-coupled inductor and voltage multiplier module," *International Journal of Power Electronics and Drive Systems*, vol. 13, no. 3, pp. 1599–1604, 2022, doi: 10.11591/ijpeds.v13.i3.pp1599-1604.

[15] H. Attia and A. Elkhatib, "Intelligent maximum power point tracker enhanced by sliding mode control," *International Journal of Power Electronics and Drive Systems*, vol. 13, no. 2, pp. 1037–1046, 2022, doi: 10.11591/ijpeds.v13.i2.pp1037-1046.

[16] A. A. M. Faudzi, S. F. Toha, R. A. Hanifah, N. F. Hasbullah, and N. A. Kamisan, "An interleaved DC charging solar system for electric vehicle," *International Journal of Power Electronics and Drive Systems*, vol. 12, no. 4, pp. 2414–2422, 2021, doi: 10.11591/ijpeds.v12.i4.pp2414-2422.

[17] K. Mohammad, M. Ahmad, S. A. Farooqui, W. Ali, and F. Khan, "Performance evaluation of a PMDC motor with battery storage control and MPPT based solar photovoltaic system," *International Journal of Power Electronics and Drive Systems*, vol. 13, no. 3, pp. 1704–1712, 2022, doi: 10.11591/ijpeds.v13.i3.pp1704-1712.

[18] M. Ouremchi, S. E. Mouzouade, K. E. Khadiri, A. Tahiri, and H. Qjidaa, "Integrated energy management converter based on maximum power point tracking for photovoltaic solar system," *International Journal of Electrical and Computer Engineering*, vol. 12, no. 2, pp. 1211–1222, 2022, doi: 10.11591/ijece.v12i2.pp1211-1222.

[19] W. Obaid, A. K. Hamid, C. Ghenai, and M. E. H. Assad, "Design of a thermoelectric energy source for water pumping applications: a case study in Sharjah, United Arab Emirates," *International Journal of Electrical and Computer Engineering*, vol. 11, no. 6, pp. 4751–4758, 2021, doi: 10.11591/ijece.v11i6.pp4751-4758.

[20] N. A. M. Aseri *et al.*, "Comparison of meta-heuristic algorithms for fuzzy modelling of Covid-19 illness' severity classification," *IAES International Journal of Artificial Intelligence (IJ-AI)*, vol. 11, no. 1, pp. 50–64, Mar. 2022, doi: 10.11591/ijai.v11.i1.pp50-64.

[21] F. A. Izzaqi, N. A. Windarko, and O. A. Qudsi, "Minimization of total harmonic distortion in neutral point clamped multilevel inverter using grey wolf optimizer," *International Journal of Power Electronics and Drive Systems*, vol. 13, no. 3, pp. 1486–1497, 2022, doi: 10.11591/ijpeds.v13.i3.pp1486-1497.

[22] M. Zadehbagheri, T. Sutikno, and R. Ildarabadi, "Using y-source network as a connector between turbine and network in the structure of variable speed wind turbine," *International Journal of Power Electronics and Drive Systems*, vol. 12, no. 3, pp. 1644–1658, 2021, doi: 10.11591/ijpeds.v12.i3.pp1644-1658.

[23] E. Najafi, A. H. Rashidi, and S. M. Dehghan, "Z-source reversing voltage multilevel inverter for photovoltaic applications with inherent voltage balancing," *International Journal of Power Electronics and Drive Systems*, vol. 13, no. 1, pp. 267–274, 2022, doi: 10.11591/ijpeds.v13.i1.pp267-274.

[24] C. A. R.-Paja, D. G.-Motoya, J. P. V.-Ceballos, S. I. S.-Garcés, and R. Giral, "Sliding-mode controller for a photovoltaic system based on a Cuk converter," *International Journal of Electrical and Computer Engineering*, vol. 11, no. 3, pp. 2027–2044, 2021, doi: 10.11591/ijece.v11i3.pp2027-2044.

[25] A. K. Kolluru and M. K. Kumar, "Artificial neural network vector controlled common high-side switch asymmetric converter fed switched reluctance motor drive," *Indonesian Journal of Electrical Engineering and Computer Science*, vol. 24, no. 2, pp. 697–703, 2021, doi: 10.11591/ijeecs.v24.i2.pp697-703.

[26] W. T. Chew, W. V. Yong, J. S. L. Ong, J. H. Leong, and T. Sutikno, "Dynamic simulation of three-phase nine-level multilevel inverter with switching angles optimized using nature-inspired algorithm," *International Journal of Power Electronics and Drive Systems*, vol. 12, no. 1, pp. 325–333, 2021, doi: 10.11591/ijpeds.v12.i1.pp325-333.

[27] M. R. J. A.-Hiealy, M. S. B. A. M. Shikh, A. B. Jalil, S. A. Rahman, and M. Jarrah, "Management switching angles real-time prediction by artificial neural network," *Indonesian Journal of Electrical Engineering and Computer Science*, vol. 23, no. 1, pp. 110–119, 2021, doi: 10.11591/ijeecs.v23.i1.pp110-119.

[28] Y. Chen and K. M. Smedley, "A cost-effective single-stage inverter with maximum power point tracking," *IEEE Transactions on Power Electronics*, vol. 19, no. 5, pp. 1289–1294, 2004, doi: 10.1109/TPEL.2004.833458.

[29] W. Libo, Z. Zhengming, and L. Jianzheng, "A single-stage three-phase grid-connected photovoltaic system with modified MPPT method and reactive power compensation," *IEEE Transactions on Energy Conversion*, vol. 22, no. 4, pp. 881–886, Dec. 2007, doi: 10.1109/TEC.2007.895461.

[30] Patel H. and Agarwal V., "Investigations into the performance of photovoltaics-based active filter configurations and their control schemes under uniform and non-uniform radiation conditions," *IET Renewable Power Generation*, vol. 4, no. 1, pp. 12–22, 2010, [Online]. Available: <https://digital-library.theiet.org/content/journals/10.1049/iet-rpg.2008.0081>

[31] T. F. Wu, H. S. Nien, H. M. Hsieh, and C. L. Shen, "PV power injection and active power filtering with amplitude-clamping and amplitude-scaling algorithms," *IEEE Transactions on Industry Applications*, vol. 43, no. 3, pp. 731–741, 2007, doi: 10.1109/TIA.2007.895764.

[32] R. K. Varma, S. A. Rahman, and T. Vanderheide, "New control of PV solar farm as STATCOM (PV-STATCOM) for increasing grid power transmission limits during night and day," in *2014 IEEE PES T&D Conference and Exposition*, 2014, pp. 755–763, doi: 10.1109/TDC.2014.6863257.

[33] R. K. Varma and E. M. Siavashi, "PV-STATCOM: a new smart inverter for voltage control in distribution systems," in *2018 IEEE Power & Energy Society General Meeting (PESGM)*, 2018, pp. 1–12, doi: 10.1109/PESGM.2018.8586325.

[34] T. Abdelwahed, M. Radouane, A. Mohamed, and R. Nabil, "Active filtering capability based on the RSC control of WECS equipped with a DFIG," *Indonesian Journal of Electrical Engineering and Computer Science*, vol. 23, no. 2, pp. 760–771, 2021, doi: 10.11591/ijeecs.v23.i2.pp760-771.

[35] M. M. E.-Sotouhy, A. A. Mansour, M. I. Marei, A. M. Zaki, and A. A. E.-Sattar, "Four-leg active power filter control with SUI-PI controller," *International Journal of Electrical and Computer Engineering*, vol. 11, no. 4, pp. 2768–2778, 2021, doi:

10.11591/ijcce.v1i14.pp2768-2778.

[36] H. V. Gururaja Rao, R. C. Mala, and A. Joshi, "Motor side active power filter for induction motor," *International Journal of Power Electronics and Drive Systems*, vol. 11, no. 4, pp. 1711–1718, 2020, doi: 10.11591/ijpeds.v11.i4.pp1711-1718.

[37] I. Alhamrouni, F. N. Hanafi, M. Salem, N. H. A. Rahman, A. Jusoh, and T. Sutikno, "Design of shunt hybrid active power filter for compensating harmonic currents and reactive power," *Telkomnika (Telecommunication Computing Electronics and Control)*, vol. 18, no. 4, pp. 2148–2157, 2020, doi: 10.12928/TELKOMNIKA.V18I4.15156.

[38] U. M. Soomro, S. K. Alsawed, M. N. B. Abdullah, N. H. B. M. Radzi, and M. H. Baloch, "Optimal design of a single-phase apf based on pq theory," *International Journal of Power Electronics and Drive Systems*, vol. 11, no. 3, pp. 1360–1367, 2020, doi: 10.11591/ijpeds.v11.i3.pp1360-1367.

[39] B. R. Madhu, M. N. Dinesh, T. Thinalas, and D. Menezes, "Enhancement of power quality using microprocessor based shunt active power filter for unbalanced load," *International Journal of Electrical and Computer Engineering*, vol. 10, no. 4, pp. 3393–3402, 2020, doi: 10.11591/ijece.v10i4.pp3393-3402.

[40] U. Sultana, S. H. Qazi, N. Rasheed, and M. W. Mustafa, "Performance analysis of real-time PSO tuned PI controller for regulating voltage and frequency in an AC microgrid," *International Journal of Electrical and Computer Engineering*, vol. 11, no. 2, pp. 1068–1076, 2021, doi: 10.11591/ijcce.v11i2.pp1068-1076.

[41] E. Radwan, M. Nour, A. Baniyounes, and K. S. A.-Olimat, "Design of type-1 servo controller for grid voltage modulated direct-power control of single-phase grid-connected PV inverter," *International Journal of Electrical and Computer Engineering*, vol. 11, no. 3, pp. 1912–1923, 2021, doi: 10.11591/ijece.v11i3.pp1912-1923.

[42] Q. Salem and K. Alzaareer, "Detailed analysis of grid connected and islanded operation modes based on p/u and q/f droop characteristics," *International Journal of Power Electronics and Drive Systems*, vol. 12, no. 2, pp. 772–782, 2021, doi: 10.11591/ijpeds.v12.i2.pp772-782.

[43] K. Odo, C. Ohanu, I. C.-Ogbuka, A. Ajibo, C. Ogbuka, and E. Ejiogu, "A novel direct torque and flux control of permanent magnet synchronous motor with analytically-tuned pi controllers," *International Journal of Power Electronics and Drive Systems*, vol. 12, no. 4, pp. 2103–2112, 2021, doi: 10.11591/ijpeds.v12.i4.pp2103-2112.

[44] B. O. Akinloye and E. S. Obe, "Performance analysis of single-phase interior permanent magnet synchronous motor," *International Journal of Power Electronics and Drive Systems*, vol. 13, no. 2, pp. 812–824, 2022, doi: 10.11591/ijpeds.v13.i2.pp812-824.

[45] A. H. Shallal, S. A. Salman, and A. H. Sabry, "Hall sensor-based speed control of a 3-phase permanent-magnet synchronous motor using a field-oriented algorithm," *Indonesian Journal of Electrical Engineering and Computer Science*, vol. 27, no. 3, pp. 1366–1374, 2022, doi: 10.11591/ijeecs.v27.i3.pp1366-1374.

[46] A. S. A.-Khayyat, A. A.-Safi, and M. J. Hameed, "Single-phase grid-connected power control in dq synchronous reference frame with space vector modulation using FPGA," *Indonesian Journal of Electrical Engineering and Computer Science*, vol. 30, no. 1, pp. 57–69, 2023, doi: 10.11591/ijeecs.v30.i1.pp57-69.

[47] M. Sujith, G. Vijayakumar, D. B. Pardeshi, S. Madhubalan, and K. G. Kannan, "PSO based optimized PI controller design for hybrid active power filter," *International Journal of Power Electronics and Drive Systems*, vol. 14, no. 2, pp. 863–871, 2023, doi: 10.11591/ijpeds.v14.i2.pp863-871.

[48] S. Swathi, B. S. Kumar, and J. Upendar, "Voltage and frequency stabilization by fuzzy integrated droop control of a multi renewable source micro grid," *Indonesian Journal of Electrical Engineering and Computer Science*, vol. 30, no. 3, pp. 1308–1320, 2023, doi: 10.11591/ijeecs.v30.i3.pp1308-1320.

[49] A. A.-Safi, "ECG signal denoising using a novel approach of adaptive filters for real-time processing," *International Journal of Electrical and Computer Engineering*, vol. 11, no. 2, pp. 1243–1249, 2021, doi: 10.11591/ijcce.v11i2.pp1243-1249.

[50] N. Beniwal, I. Hussain, and B. Singh, "Hybrid VSS–LMS–LMF based adaptive control of SPV-DSTATCOM system under distorted grid conditions," *IET Renewable Power Generation*, vol. 12, no. 3, pp. 311–322, 2018, doi: 10.1049/iet-rpg.2016.0868.

[51] S. Chintala, J. Thangaraj, and D. R. Edla, "Elimination of EOG signals from raw EEG signals using step size based recursive least squares- least mean fourth adaptive algorithm," *Applied Acoustics*, vol. 180, p. 108097, 2021, doi: 10.1016/j.apacoust.2021.108097.

[52] S. Singh, V. Narayanan, B. Singh, and B. K. Panigrahi, "Two-stage 3-Φ utility interfaced PV-BES with synchronization capability," in *2022 IEEE Global Conference on Computing, Power and Communication Technologies (GlobConPT)*, 2022, pp. 1–6, doi: 10.1109/GlobConPT57482.2022.9938273.

[53] B. Singh and J. Solanki, "A comparison of control algorithms for DSTATCOM," *IEEE Transactions on Industrial Electronics*, vol. 56, no. 7, pp. 2738–2745, 2009, doi: 10.1109/TIE.2009.2021596.

[54] A. Abdulmula *et al.*, "Micropower system optimization for the telecommunication towers based on various renewable energy sources," *International Journal of Electrical and Computer Engineering*, vol. 12, no. 2, pp. 1069–1076, 2022, doi: 10.11591/ijcce.v12i2.pp1069-1076.

[55] M. Annoukoubi, A. Essadki, H. Laghrifat, and T. Nasser, "Reduction of harmonics emission of a WECS in the electrical grid using multilevel inverters," *International Journal of Power Electronics and Drive Systems*, vol. 13, no. 3, pp. 1519–1536, 2022, doi: 10.11591/ijpeds.v13.i3.pp1519-1536.

[56] H. Essakhi, S. Farhat, Y. Dbaghi, and D. Daou, "Indirect power control of grid-connected photovoltaic system using fuzzy control with a three-level inverter," *Indonesian Journal of Electrical Engineering and Computer Science*, vol. 28, no. 1, pp. 76–87, 2022, doi: 10.11591/ijeecs.v28.i1.pp76-87.

[57] N. Shrivastava and A. Bailyan, "Analysis of fractional order systems using newton iteration-based approximation technique," *International Journal of Electrical and Computer Engineering*, vol. 13, no. 1, pp. 116–124, 2023, doi: 10.11591/ijcce.v13i1.pp116-124.

[58] O. Barki, Z. Guennoun, and A. Addaim, "New approach for selecting multi-point relays in the optimized link state routing protocol using self organizing map artificial neural network: OLSR-SOM," *IAES International Journal of Artificial Intelligence*, vol. 12, no. 2, pp. 648–655, 2023, doi: 10.11591/ijai.v12.i2.pp648-655.

[59] T. O. Araoye *et al.*, "Modeling and optimization of hybrid microgrid energy system: a case study of University of Abuja, Nigeria," *International Journal of Power Electronics and Drive Systems*, vol. 14, no. 2, pp. 1201–1209, 2023, doi: 10.11591/ijpeds.v14.i2.pp1201-1209.

[60] H. Akagi, E. H. Watanabe, and M. Arede, *Instantaneous power theory and applications to power conditioning*. New Jersey, USA: John Wiley & Sons, 2017, doi: 10.1002/97811193838.

[61] S. Bhattacharya, D. M. Divan, and B. Banerjee, "Synchronous frame harmonic isolator using active series filter," in *European conference on power electronics and applications*, 1992, p. 30.

[62] P. Tenti and P. Mattavelli, "A time-domain approach to power term definitions under non-sinusoidal conditions," in *Sixth International Workshop on Power Definitions and Measurements under Non-Sinusoidal Conditions Milano*, 2004, pp. 1–10.

[63] P. Tenti, H. K. M. Paredes, and P. Mattavelli, "Conservative power theory, a framework to approach control and accountability issues in smart microgrids," *IEEE Transactions on Power Electronics*, vol. 26, no. 3, pp. 664–673, 2011, doi: 10.1109/TPEL.2010.2093153.

[64] P. Tenti, H. K. M. Paredes, F. P. Marafão, and P. Mattavelli, "Accountability in smart microgrids based on conservative power theory," *IEEE Transactions on Instrumentation and Measurement*, vol. 60, no. 9, pp. 3058–3069, 2011, doi: 10.1109/TIM.2011.2162351.

BIOGRAPHIES OF AUTHORS



Darshni M. Shukla     received an engineer degree in Electrical Engineering from Dr. Harisingh Gour University, Saugor, India in 1995, an M. Tech in power electronics and electrical drives from SVNIT, Surat in the year, and Ph.D. from Gujarat Technological University, Gujarat in the year 2022. Currently, she is an assistant professor at Government Engineering College Surat in Department of Electrical Engineering. Her research interests include renewable energy, electrical drives, and multilevel converters. She can be contacted at email: darshnishukla@yahoo.com.



Naimish Zaveri     is a professor at the Department of Electrical Engineering, C.K. Pithawala College of Engineering & Technology Surat. He has done B. Tech. in Electrical Engineering from SVNIT Surat, India, in 1999, and an M.E. (Electrical) B.V.M, V.V. Nagar. He completed his Ph.D. in Electrical Engineering from SVNIT Surat, in 2012. His research interests are primarily in the area of power quality, renewable energy, solar photovoltaic, and active filters. Where he is the author/co-author of many research publications. He can be contacted at email: naimish.zaveri@ckpcet.ac.in.



Tole Sutikno     is currently employed as a lecturer in the Department of Electrical Engineering at Universitas Ahmad Dahlan (UAD), which is located in Yogyakarta, Indonesia. In 1999, 2004, and 2016, he graduated with a Bachelor of Engineering from Universitas Diponegoro, a Master of Engineering from Universitas Gadjah Mada, and a Doctor of Philosophy in Electrical Engineering from Universiti Teknologi Malaysia. All three degrees are in the field of electrical engineering. Since the year 2008, he has held the position of associate professor at the University of Ahmad Dahlan in Yogyakarta, Indonesia. His research interests include the areas of digital design, industrial applications, industrial electronics, industrial informatics, power electronics, motor drives, renewable energy, FPGA applications, embedded systems, artificial intelligence, intelligent control, digital libraries, and intelligent control. He can be contacted at email: tole@te.uad.ac.id.